

Vol. 80 Commemorative Accounts

Electrochemical Energy Generation and Storage. Fuel Cells and Lithium-Ion Batteries

Héctor D. Abruña,*[1,2] Futoshi Matsumoto,[1,2] Jamie L. Cohen,[1,2] Jing Jin,[1,2] Chandrani Roychowdhury,[1,2] Mark Prochaska,[2,3] R. Bruce van Dover,[2,4] Frank J. DiSalvo,[1,2] Yasuyuki Kiya,[1,5] Jay C. Henderson,[1] and Geoffrey R. Hutchison[1]

[1]Department of Chemistry and Chemical Biology, Baker Laboratory, Cornell University, Ithaca, New York 14853, U.S.A.

[2]Cornell Fuel Cell Institute, Cornell University, Ithaca, New York 14853, U.S.A.

[3]Department of Applied and Engineering Physics, Cornell University, Ithaca, Cornell University, Ithaca, New York 14853, U.S.A.

[4]Department of Materials Science and Engineering, Cornell University, Ithaca, New York 14853, U.S.A.

[5]Subaru Research and Development Inc., Ann Arbor, Michigan 48108, U.S.A.

Received April 2, 2007; E-mail: hda1@cornell.edu

We illustrate our current work for electrochemical energy generation and storage (i.e., fuel cells and lithium-ion batteries, respectively). In fuel cell research, we have been developing Pt-based ordered intermetallic compounds as electrocatalysts towards anodic reactions of liquid fuels such as methanol, ethanol, and formic acid for proton-exchange membrane fuel cells (PEMFCs). Development of the intermetallic compounds ranges from bulk materials to nanoparticles. In our work, we have employed a combinatorial method to achieve rapid screening of a large number of potential electrocatalysts. Multi-element sputtering was employed to generate films with different compositions including most of a phase diagram and the resulting libraries were screened using a fluorescence assay. For portable applications, we have also developed a planar microfluidic membraneless fuel cell (PMMFC) device, which eliminates the need for a polyelectrolyte membrane (PEM) and takes advantage of the laminar flow of fuel and oxidant streams. Particularly, in order to increase power density (cell voltages) of a PMMFC device, we have focused on the development of a dual electrolyte PMMFC in which alkaline and acid electrolyte solutions are employed for fuel and oxidant streams, respectively. In lithium-ion battery research, we have been designing new cost-effective organic materials with high energy densities as cathode electroactive materials, targeting large applications such as electrically powered automotives. In particular, we have focused on organosulfur-based polymers, involving the redox chemistry of thiolates (RS^-), capable of higher energy density than conventional lithium metal oxides such as $LiCoO_2$. By combining electrochemical techniques with computational methods and organic synthesis, we have tried to establish an efficient procedure to develop novel organic-based electroactive materials suitable for the demands of energy storage materials for rechargeable lithium-ion batteries.

1. Fuel Cells

1.1 Introduction. Today, problems arising from the depletion of fossil fuels, and air pollution arising from their burning, have captured the attention of scientists and policy makers world-wide.[1] If we do not consider a global change in which we greatly reduce the rate of use of fossil fuels, we will rapidly reach the limit of our energy production in the near future. The development of new energy sources, and improvements in energy efficiency in generation, conversion, and storage, have become some of the most pressing issues confronting today's scientific community.[2] In this context, the use of fuel cells has been presented as one of the most promising technologies. Fuel cells are devices that directly convert chemical energy into electricity, using electrochemical reactions, and can reach efficiencies as high as 90%.[2,3] Their theoretical conversion efficiencies are much higher than coal-fired power stations or the internal combustion engine because of Carnot cycle limitations. In its simplest form, a fuel cell can use hydrogen and oxygen, where hydrogen is used as a fuel and oxygen as an oxidant. The oxidation of fuel produces electrons to generate electricity with water and heat as waste products.[4] However, in the present technologies, high purity hydrogen gas is necessary. This requires expensive, heavy, and bulky fuel reformers to be incorporated into the fuel cell systems. Recently, there has been an increased interest in direct fuel cells (DFCs), within

Published on the web October 12, 2007; doi:10.1246/bcsj.80.1843

the area of polymer electrolyte membrane (PEM) fuel cells, that use small organic molecule (SOMs) liquid fuels, such as methanol, ethanol, formic acid, etc., directly without reformation to H_2. These liquid fuels have higher volumetric and gravimetric energy densities, better energy efficiencies, in addition to ease of handling of liquid fuels during storage and transfer.[5–7] In order to develop polymer electrolyte membrane direct fuel cells (PEMDFCs) which satisfy demands from both economical, and environmental, points of view and to spread the application of PEMDFCs to various areas, a number of important issues must be resolved. One is the development of electrocatalyst materials for the anode and cathode. The second is the miniaturization of fuel cells for use as portable high energy density power sources. We have addressed these issues using forward-thinking methodologies based on a multidisciplinary approach, combining electrochemistry, materials science, and micro-fabrication technologies.

In the area of catalysis, serious losses of energy due to slow oxidation kinetics of the SOMs, and gradual decreases in catalytic activity by carbon monoxide (CO) poisoning over time, occur at the anode on conventional electrocatalyst surfaces. Many researchers have attempted the improvement of electrocatalytic activity and tolerance to CO in the electro-oxidation of SOMs with Pt-based bimetallic[8] and trimetallic[9] alloys, and Pt-group metals.[10] Our approach has focused, for the first time, on ordered intermetallic phases as new electrocatalyst materials.[11,12] Orderd intermetallic phases consist of atomically ordered structures of two or more elements, and are hypothesized to show superior electrocatalytic behavior in terms of onset of fuel oxidation potential, current density, and tolerance to CO. Among the ordered intermetallic phases that have been tested, PtBi and PtPb have demonstrated higher electrocatalytic activities in formic acid (FA) oxidation, and appreciable tolerance to CO, compared to pure polycrystalline Pt. In addition, as part of this approach, ordered intermetallic nanoparticles have been also prepared.[13–16] These provide increased surface area, which, in turn, should lead to higher outputs and are more amenable, in terms of the level of the catalyst loading, for incorporating ordered intermetallic phases into actual PEMFCs. The same electrocatalytic performance observed with bulk PtBi and PtPb has also been observed using the PtBi and PtPb nanoparticles. The use of ordered intermetallic phases can be considered to represent a new paradigm in the judicious, and deliberate, development and design of new electrocatalytic materials for fuel cell applications, in contraposition to adatom-modified surfaces and bulk alloys. In addition, combinatorial methods for high throughput screening of electrocatalyst materials have been developed in order to explore promising electrocatalysts with specific and desired properties.[17] A fluorescence assay was employed to detect the regions of high activity present in such libraries.

In a second area of research, recently, there has been great emphasis on the development of micro-fuel-cell technologies. These require the ability to scale down macro-fuel-cell systems, while retaining their power generation capabilities. They are being developed as portable high energy density power sources for consumer electronics, military applications, medical diagnostic equipment, and mobile communications.[18] One of the greatest challenges involved has been the incorporation of a PEM into a micro-fuel-cell, and sustainability of its stability over time, especially under high current density operation.[19] However, it is difficult to decrease the dimensions and thickness of the PEMs without compromising its effectiveness. Therefore, we have fabricated a membraneless microchannel fuel cell platform based on laminar flow.[20] In these microchannel fuel cells, the interface between the fuel and oxidant acts as a diffusive membrane, allowing ionic transport between the fuel and oxidant streams, thus eliminating the PEM. This system provides significant advantages over present fuel cells; the elimination of the membrane itself, fuel crossover and an increase in cell voltage by employing a dual electrolyte configuration consisting of planar flow of alkaline fuel and acidic oxidant solutions, a combination that is precluded by the use of a membrane.

1.2 Ordered Intermetallic Phases vs. Alloys in the Oxidation of SOMs. Pt–Ru alloys have been used extensively as anode electrocatalysts in PEM direct fuel cells, particularly with methanol as fuel. Indeed, in the oxidation of methanol, Pt–Ru alloys have shown better tolerance to CO poisoning, increased current densities, and a decreased overpotential for fuel oxidation when compared to pure Pt.[21] The activity of Pt–Ru alloys is ascribed to an oxygenated species generated from the dissociation of water at Ru sites at low potentials relative to the analogous processes on Pt.[22] These oxygenated surface species accelerate the oxidation of CO to CO_2 and thus remove adsorbed CO from Pt sites at lower potentials than at pure Pt surfaces through the so-called bifunctional mechanism. Because of these properties, Pt–Ru alloys have been among the most promising catalysts for direct fuel cells in the past few decades, especially for methanol oxidation. Pd and Pt–Pd alloys have also been reported to exhibit an enhancement in reactivity towards FA oxidation.[23] However, a slow deactivation, due to surface oxidation of Pd, causes a diminution of the oxidation current over time during the oxidation of FA. This instability of the Pd surface is one disadvantage of using Pd as an anode catalyst in direct FA fuel cells. Pt–Pd alloys show a trend opposite to that observed for Pt–Ru for adsorption of CO on the surface. The peak potential for CO stripping on Pt–Pd surfaces appears at values higher than at a Pt surface, indicating that CO binds more strongly to Pt–Pd than to pure Pt. This leads to the conclusion that FA oxidation on Pt–Pd surfaces favors the direct formation of CO_2 without the formation of CO, that is to say, the path leading to CO appears to be precluded. Although the aforementioned alloys are promising materials, there exist other problems with the application of disordered Pt–Ru and Pt–Pd alloys (and alloys in general) as catalysts for fuel cell applications. For example, low utilization of the surface for electrocatalysis, surface segregation of metal atoms, and partial poisoning by CO and sulfur-containing compounds because of inherently poor definition of alloy surface structures with surface sites occupied by Pt or Ru in a random fashion (Figs. 1a and 1c). The use of Ru-based alloys in place of pure Pt introduces a stability problem: during extended periods of operation, particularly under non-optimal usage (especially at high temperatures and current densities), the alloy surface becomes depleted of Ru. Ru has a higher surface energy than Pt, and will eventually migrate into the bulk.[23]

In order to mitigate some of the above-mentioned issues

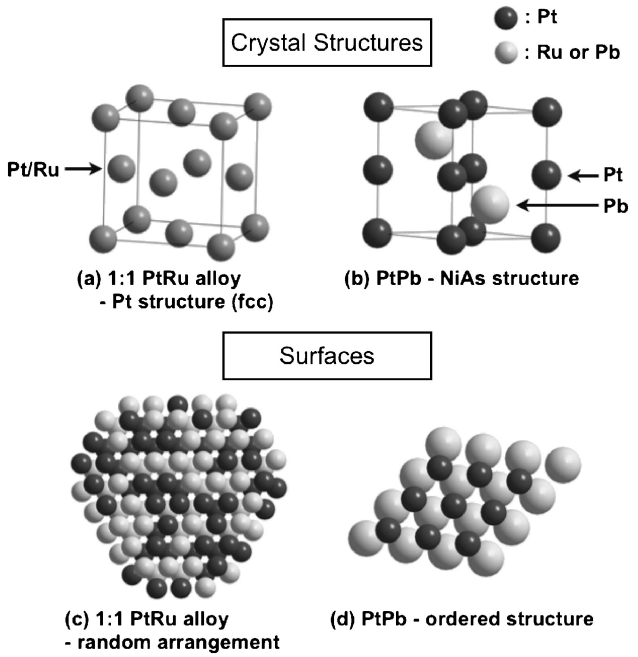

Fig. 1. Crystal (a and b) and surface (c and d) structures of 1:1 Pt–Ru alloy (a and c) and PtPb-ordered intermetallic phase (b and d).

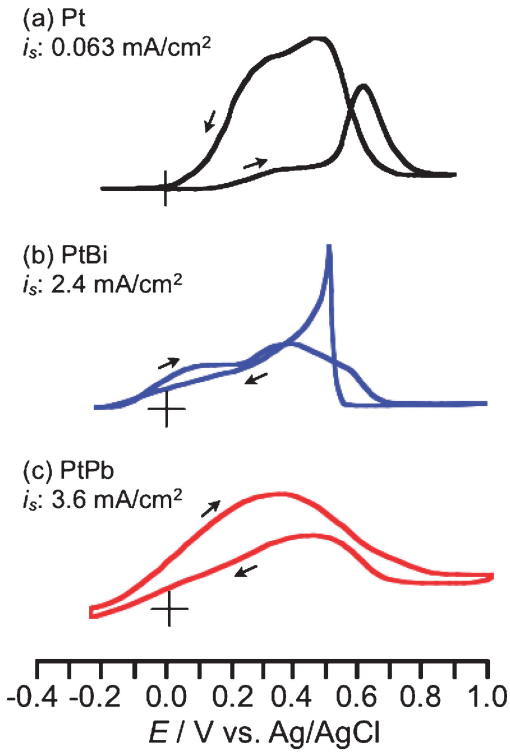

Fig. 2. Cyclic voltammograms (CVs) for (a), (b) 0.125 M and (c) 0.250 M formic acid (FA) solutions at (a) Pt, (b) PtBi, and (c) PtPb in 0.1 M H_2SO_4. Scan rate was 10 mV s^{-1}.

associated with alloy catalysis, ordered intermetallic structures are being investigated. In ordered intermetallic phases, all atoms on the surface have the same local geometry (Figs. 1b and 1d).[11] In addition, although pure Bi and Pb metals will easily leach out at much lower potentials, intermetallic compounds are capable of stabilizing Bi and Pb atoms against electrochemical dissolution. That is, the free energy (ΔG^0_f) of formation for the PtPb ordered intermetallic phase is approximately $-51\,kJ\,mol^{-1}$. Thus, this represents a shift in the onset potential of $\Delta E = +260\,mV$ so that the $E^{0'}$ value for PtPb is +0.13 V, which implies that PtPb is stable at low pH. On the other hand, there is virtually no stabilization of Ru against dissolution by alloy formation on PtRu because $\Delta G^0_f \approx 0$ in a PtRu alloy. In addition, PtBi- and PtPb-ordered intermetallic phases have shown a dramatic diminution in the affinity of CO that make them amenable to use in the presence of CO at levels that would poison Pt and PtRu alloy catalysts. We have investigated the properties of ordered intermetallic compounds as a means to improve the performance of anode materials for fuel cell applications.

In order to further understand the electrochemical behavior of ordered intermetallic phases with respect to the oxidation of a variety of potential fuels, we have studied the electrocatalytic activity of a wide range of bulk ordered intermetallic phases and the results have been compared to those of a pure polycrystalline Pt electrode.[11,12] Among those studied, PtBi- and PtPb-ordered intermetallic bulk phases, in particular, have exhibited remarkable electrocatalytic activity for the oxidation of FA in terms of onset potential and current density (Fig. 2b). The PtBi phases showed an onset of oxidation potential (−0.12 V), approximately 300 mV more negative than pure Pt (Fig. 2a). The steady-state current density (i_s) of the PtBi phases is 40 times larger than that of pure Pt in the oxidation of FA. Moreover, the oxidation of FA observed at PtPb (Fig. 2c) showed a further negative onset potential shift and increased steady-state current density, compared to PtBi. These results indicate that ordered intermetallic phases represent a viable venue to find suitable electrocatalysts for fuel cell applications.

CO is known to be among the most deleterious poisons in direct-type PEM fuel cells using SOMs as fuels. The CO intermediate species strongly adsorbs onto the Pt atoms blocking the oxidation of FA and methanol at these sites. Eliminating the CO intermediate and inhibiting its adsorption are some of the major factors in achieving high anode performance. Therefore, electrocatalysts that are tolerant to CO are desired in order to realize high conversion efficiency and long term activity. Following CO adsorption, the Pt surface shows no current up to about +0.65 V and a sharp peak about +0.65 V ascribed to the oxidation of adsorbed CO to CO_2 (Fig. 3b).[11] On the other hand, the effect of CO exposure to PtBi-ordered intermetallic phases is shown in Fig. 3c and differs dramatically from Pt. The voltammograms remained essentially unchanged before and after CO exposure, indicating that CO molecules do not irreversibly adsorb on the surface of the PtBi-ordered intermetallic. The dramatic drop in the adsorption of CO on the PtBi-ordered imtermetallic surface is considered to be, at least in part, a direct consequence of its structure, specifically, the difference in the Pt–Pt distance between bulk Pt (and alloys) and PtBi. The expansion of the Pt–Pt distance in PtBi (from 2.78 to 4.32 Å; the latter for PtBi in the [001] direction) makes it very difficult for CO to bind in bridge or three-fold hollow site configurations on PtBi.

1.3 Synthesis, Characterization, and Electrocatalytic

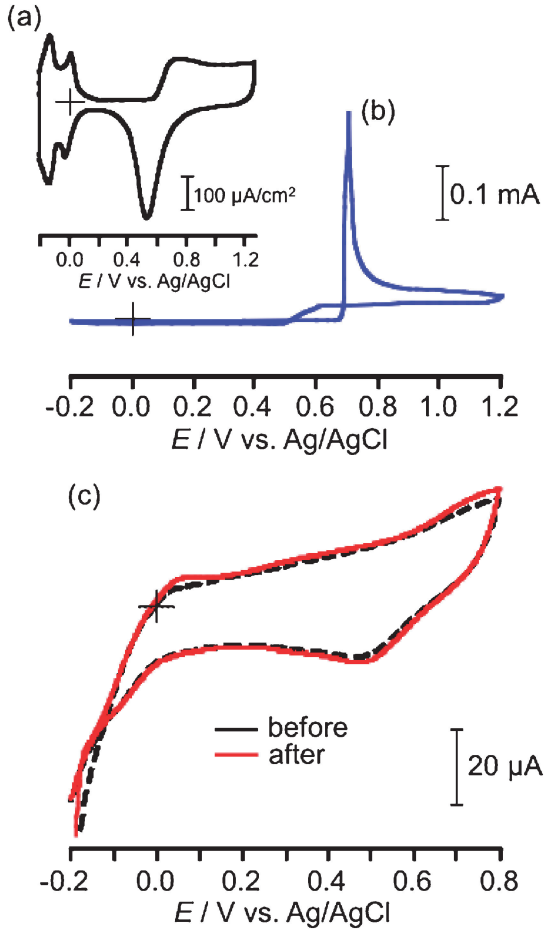

Fig. 3. CVs for 0.1 M H_2SO_4 solutions at a Pt electrode (a) before and (b) after exposure to CO. Scan rate was 50 mV s^{-1}. (c) CVs for 0.1 M H_2SO_4 solutions at a PtBi electrode before and after exposure to CO. Scan rate was 10 mV s^{-1}.

Activities of Ordered Intermetallic Phases in Nanoparticle Form. We have prepared nanoparticles of ordered intermetallic phases by reacting metal precursors salts with strongly reducing agents at room temperature.[13–16] For example, we prepared PtPb-ordered intermetallic nanoparticles with $H_2PtCl_6 \cdot 6H_2O$, $Pb(C_2H_3O_2)_2 \cdot 3H_2O$, and sodium borohydride ($NaBH_4$). The BET surface area of these PtPb nanoparticles was 15 $m^2\,g^{-1}$.[15] In addition, the pXRD pattern (Fig. 4a) of the PtPb nanoparticles showed the formation of single-phase-ordered intermetallic PtPb with an average grain size of 12 nm. Bright field STEM images of the synthesized PtPb nanoparticles (Fig. 4b) showed the individual particles to be about 15–30 nm in size and which aggregated to form networks. When the activity of the PtPb nanoparticles was compared to that of commercially available Pt and Pt–Ru alloy nanoparticles for the oxidation of FA, the PtPb nanoparticles showed remarkably superior electrocatalytic activity in terms of oxidation onset potential (−0.2 V vs. Ag/AgCl) and current density (2.94 mA cm^{-2} at +0.2 V).[15]

Long-term electrocatalytic activity of the PtPb nanoparticles has also been investigated by chronoamperometry in the oxidation of FA at constant potentials (Fig. 5). The stability of the oxidation current of the PtPb nanoparticles (a) was compared

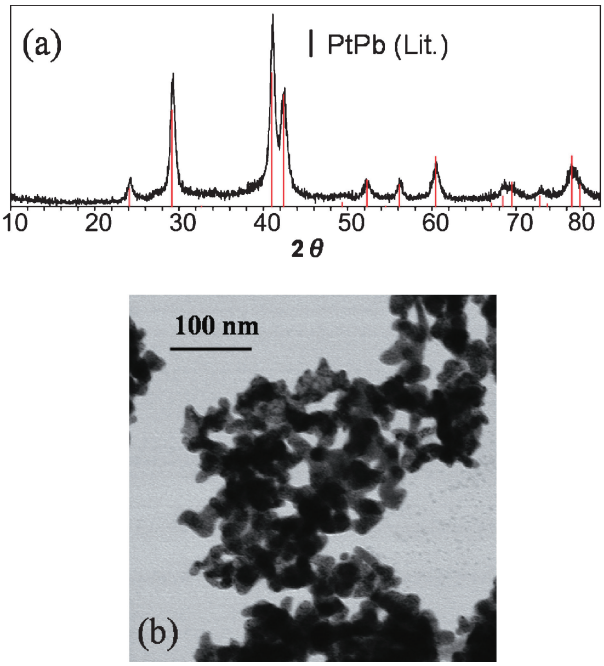

Fig. 4. pXRD pattern (a) and STEM image (b) of PtPb nanoparticles prepared by reducing H_2PtCl_6 and $Pb(C_2H_3O_2)_2$ with $NaBH_4$ [Reprinted with permission from L. R. Alden, C. Roychowdhury, F. Matsumoto, D. K. Han, V. B. Zeldovich, H. D. Abruña, F. J. Disalvo, *Langmuir* **2006**, *22*, 10465. Copyright 2006, American Chemical Society.].

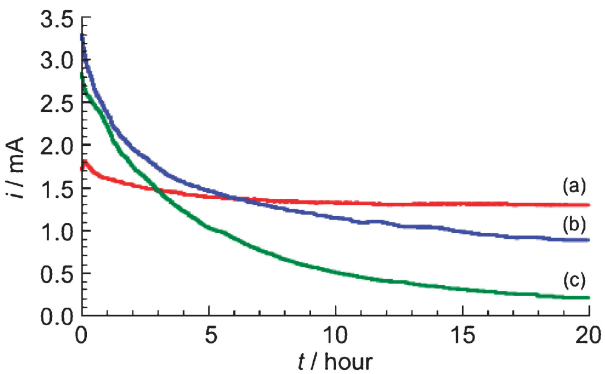

Fig. 5. Time-dependences of the oxidation current for a 0.5 M FA solution obtained at (a) PtPb-ordered intermetallic nanoparticle (average grain size: 12 nm), (b) Pt–Ru alloy, and (c) Pt black nanoparticles (loading 0.25 mg cm^{-2})-coated rotating glassy carbon electrodes (GCEs, 3 mm diameter) in 0.1 M H_2SO_4 at 3600 rpm. The changes in the oxidation currents were observed at (a) 0.0 and (b,c) +0.4 V, respectively.

with those of a PtRu alloy (b) and Pt black (c) nanoparticles. While Pt black and PtRu alloy nanoparticles rapidly deteriorated from 2.5–3.5 mA down to less than 1 mA during the oxidation at +0.4 V, PtPb nanoparticles exhibited a stable oxidation current of 1.3 mA during oxidation at 0.0 V. for over 20 h, indicating the stability of the PtPb nanoparticle catalysts. The rapid decrease in the FA oxidation current observed on the Pt and PtRu nanoparticles is likely due to poisoning by

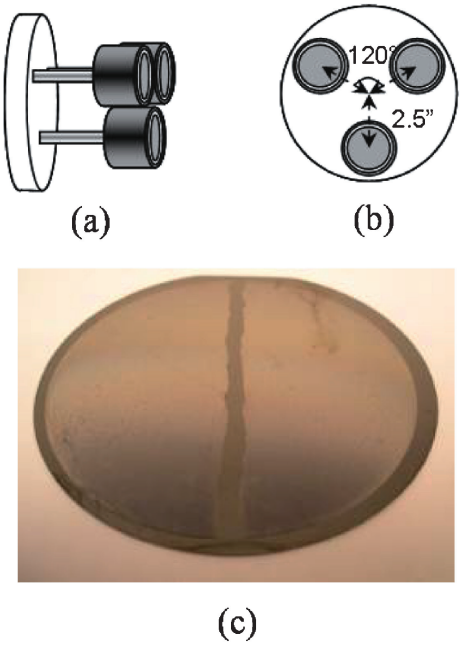

Fig. 6. (a) Schematic depiction of the three sputter-guns. (b) A front view of the triangular array of sputter guns. Each gun is positioned 2.5 inch from the center of the flange and 120° apart. (c) A substrate prepared for deposition profile analysis [Reprinted with permission from M. Prochaska, J. Jin, D. Rochefort, L. Zhuang, F. J. DiSalvo, H. D. Abruña, R. B. van Dover, *Rev. Sci. Instrum.* **2006**, *77*, 054104/1. Copyright 2006, American Institute of Physics.].

CO, which is the main intermediate species formed during the FA oxidation reaction. In fact, after electrolysis of FA for 20 h, the Pt and Pt–Ru nanoparticles showed a sharp CO stripping peak in 0.1 M H_2SO_4 solution consistent with this assertion. On the other hand, the PtPb nanoparticles did not show a CO stripping peak in a 0.1 M H_2SO_4 solution even after electrolysis for 20 h.

1.4 High-Throughput Screening of Electrocatalyst Materials with Combinatorial Libraries. We have employed multi-element sputtering to generate films with different compositions that include most of a phase diagram and have screened the generated libraries using a fluorescence assay based on quinine.[17] In our combinatorial method, thin-film ternary composition spreads were generated in a cylindrical vacuum chamber with three sputter-guns inserted horizontally into a circular flange (Figs. 6a and 6b). The guns were arranged at the vertices of an equilateral triangle (120°), 2.5 inches from the center of the flange. The composition spreads are designed to have a 1:1:1 molar ratio of the three elements at the center of the substrate as shown in Fig. 6c. Interdiffusion of elements allows compound, alloy and ordered intermetallic phases formation.

Figures 7a–7d shows a sequence of fluorescence images obtained at various applied potentials in 5 M methanol, 0.1 M CF_3SO_3Na, and 0.5 mM quinine and an X-ray diffraction pattern (Fig. 7e) obtained from spot 1 shown in Fig. 7d, where fluorescence was initially detected. At the initial potential of 0 V (vs. Ag/AgCl), no fluorescence was observed. At an applied potential of +0.20 V, there is a faint fluorescent spot near the intersection of the Pt/Pb-rich regions. At +0.25 V, the fluorescence intensity from the spot is greatly enhanced. The X-ray diffraction pattern obtained at the spot where fluorescence was initially observed indicated that the material had a simple phase NiAs structure type. Microprobe analysis with energy dispersive spectroscopy (EDS) indicated that the material with a composition of $Pt_{0.38}(Bi/Pb)_{0.62}$ was the most active in methanol oxidation. On the other hand, spot 2 in Fig. 7d did not exhibit any electrocatalytic activity even at an applied potential of +0.25 V even though this region was physically proximate to the most active spot. This type of analysis might be of great help in understanding reactivity–structure relationships. Furthermore, it made clear that our approach allows

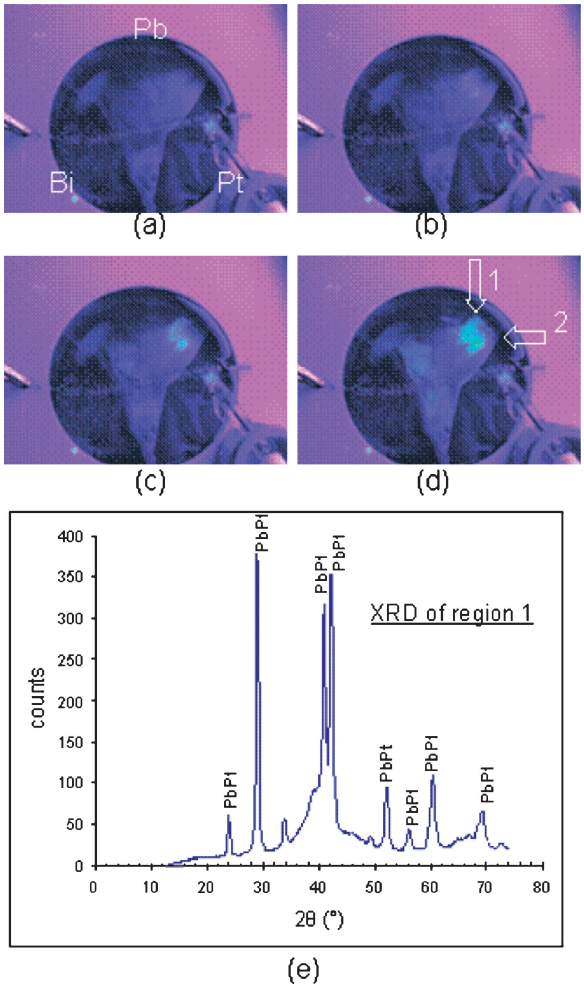

Fig. 7. Fluorescence images of the composition spread of Pt, Bi, and Pb at different applied potential in methanol oxidation in 5 M methanol, 0.1 M CF_3SO_3Na, and 0.5 mM quinine aqueous solution. (a) $E = 0$ V, (b) $E = +0.15$ V, (c) $E = +0.20$ V, (d) $E = +0.25$ V (vs. Ag/AgCl). (e) XRD data of the active region 1. The orientation of the three sputtering guns relative to the spread is shown in (a) [Reprinted with permission from M. Prochaska, J. Jin, D. Rochefort, L. Zhuang, F. J. DiSalvo, H. D. Abruña, R. B. van Dover, *Rev. Sci. Instrum.* **2006**, *77*, 054104/1. Copyright 2006, American Institute of Physics.].

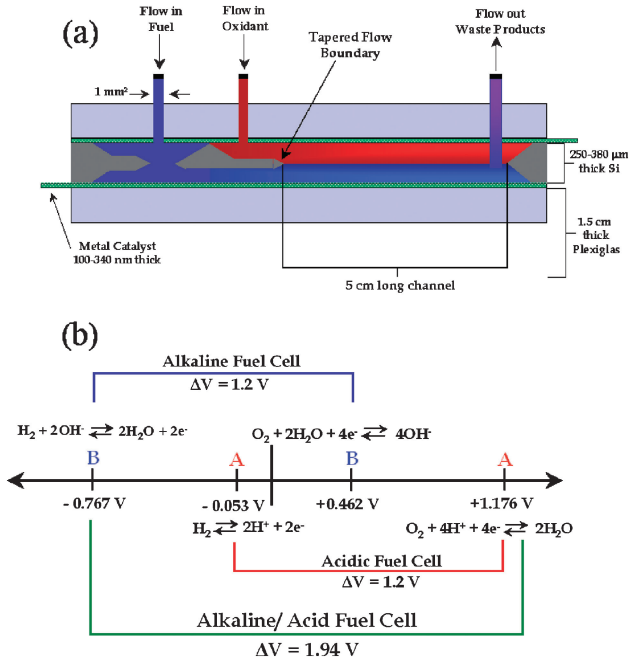

Fig. 8. (a) Side view of the planar microfluidic membraneless fuel cell and (b) thermodynamic considerations of H_2/O_2 systems. The acid employed is 0.1 M H_2SO_4 (pH 0.9) and the base is 0.1 M KOH (pH 13). Potentials versus standard hydrogen electrode (SHE) [Reprinted with permission from J. L. Cohen, D. J. Volpe, D. A. Westly, A. Pechenik, H. D. Abruña, *Langmuir* **2005**, *21*, 3544. Copyright 2005, American Chemical Society.].

for rapid screening and preliminary identification of promising materials.

1.5 Development of a Dual Electrolyte Planar Membraneless Microchannel Fuel Cells with High Open Circuit Potential. Planar membraneless microchannel fuel cells (PMMFC) based on laminar flow of fuel and oxidant streams between two parallel-plate electrodes have been fabricated. The planar anode and cathode electrodes allow for increased power generation due to the large contact area between the fuel and oxidant and the electrode surfaces. Our approach is based on the use of what we term a "tapered flow boundary" (Fig. 8a) designed to establish a condition of laminar flow of two solution streams flowing on either side of the boundary prior to coming into contact.[20] Fuel crossover is essentially eliminated because the solutions mix only by diffusion at their interface. Moreover, in order to increase the cell voltage, a dual electrolyte PMMFC can be considered by using H_2 as a fuel dissolved in 0.1 M KOH and O_2 as an oxidant dissolved in 0.1 M H_2SO_4.[24] As shown in Fig. 8b, the thermodynamic open circuit cell potential of H_2/O_2 in acid or alkaline electrolyte systems is 1.23 V when calculated using 0.1 M H_2SO_4 (pH 0.9) for the acid and 0.1 M KOH (pH 13) for the base with concentrations of 1 mM for H_2 and O_2. The dual electrolyte PMMFC with H_2 dissolved in an aqueous alkaline solution and O_2 dissolved in an aqueous acid solution has a thermodynamically calculated open circuit cell potential of 1.94 V. This is 0.71 V greater than that calculated for acid, or alkaline, single electrolyte systems as described above.

Figure 9 presents the power results for a five-microchannel

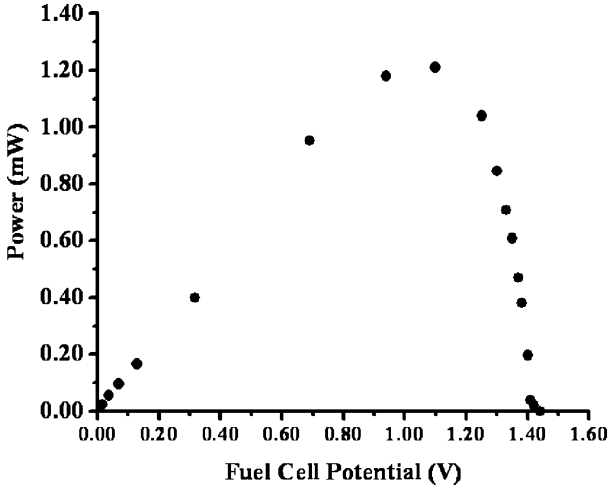

Fig. 9. Power results for a five-microchannel (each 1 mm wide, 250 mm thick) array. Kapton® electrodes of 50 nm of Ta and 50 nm of Pt were used. Fuel and oxidant were 0.1 M KOH saturated with H_2 and 0.1 M H_2SO_4 saturated with O_2, respectively. The flow rate was 4.0 mL min^{-1} [Reprinted with permission from J. L. Cohen, D. J. Volpe, D. A. Westly, A. Pechenik, H. D. Abruña, *Langmuir* **2005**, *21*, 3544. Copyright 2005, American Chemical Society.].

array of a planar microfluidic membraneless fuel cell, in which the fuel was H_2/0.1 M KOH and the oxidant was O_2/0.1 M H_2SO_4. The total power generated was 1.2 mW. An open-circuit cell potential in excess of 1.4 V was achieved with the dual electrolyte system. This is a 500 mV increase in the open circuit cell potential observed for single electrolyte H_2/O_2 systems. The dual electrolyte fuel cell systems showed power generation of 0.6 mW cm^{-2} from a single device, which is nearly 0.25 mW cm^{-2} greater than the values obtained for single electrolyte H_2/O_2 fuel cell systems.

2. Lithium-Ion Batteries (LIBs)

2.1 Introduction. Lithium-ion batteries (LIBs) are considered as one of the most important energy-devices since they have the highest energy density of all secondary batteries. As a result, they are used in a wide range of applications from cellular phones to automotives.[4,25,26] Since commercialization of the first lithium-ion rechargeable battery by SONY in 1990, intercalation compounds such as metal oxides[26–28] ($LiCoO_2$, $LiMnO_2$, $LiNiO_2$, etc.) and metal phosphates[26,29,30] ($LiFePO_4$, $LiMnPO_4$, etc.) have received a great deal of attention as cathode electroactive materials. As a general class, they can provide gravimetric capacities (storable charge per unit mass) of ca. 120–160 mA h g^{-1}. On the other hand, anode electroactive materials[31–35] such as graphite, silicon, tin oxides, metal oxides, and lithium metal possess much higher gravimetric capacities (ca. 370–3860 mA h kg^{-1}) when compared to the cathode materials. Thus, in order to achieve further enhancements in the energy density of lithium-ion batteries, it is imperative to improve the cathode performance. Furthermore, it is also important to take into account cost and availability of electroactive materials as the LIBs markets have continued to grow and have begun targeting larger applications (i.e., pure and hybrid electric vehicles), for which large amounts of materials are required.

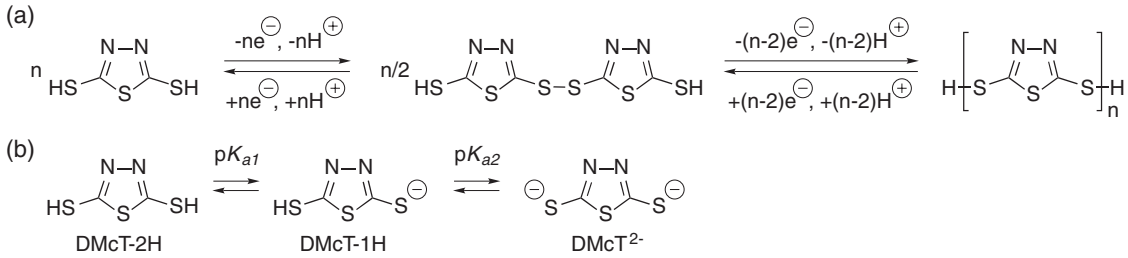

Scheme 1. Redox reactions and proton equilibria schemes for 2,5-dimercapto-1,3,4-thiadiazole (DMcT).

Organosulfur compounds with multiple thiol groups or disulfide moieties have received attention as cathode active-materials for lithium/lithium-ion rechargeable batteries due to their high theoretical capacities.[36–45] Organic materials also offer the advantage of being relatively low cost and derived from abundant resources, as opposed to the metal oxides currently employed. Moreover, chemical tunability of the compounds has made them even more attractive. In addition, the capability of the thiolate redox chemistry to release and capture lithium ions during discharge enable them to be easily incorporated into a "rocking-chair"-type system employed in lithium-ion batteries.[36] However, the practical application of these compounds has been hindered because of the sluggish kinetics of the redox reactions at room temperature and their lack of electronic conductivity. Thus, in order to realize organosulfur-based cathodes in practical lithium-ion battery applications, the sluggish redox reactions must be accelerated and sufficient electronically conductive pathways need to be established.

2.2 Electrocatalytic Effect of Conducting Polymers towards Organosulfur Compounds to Accelerate the Charge-Transfer Kinetics. To meet these requirements, our group has been focusing on the use of conducting polymers as electrocatalysts for redox reactions of organosulfur compounds.[42,46,47] Additional advantages of conducting polymers are that they possess their own redox reactions (and thus additional capacity) and exhibit electronic conductivity when they are oxidized (p-type doping) or reduced (n-type doping).[48] Therefore, they can also be used both as an electroactive material and for providing electronically conductive pathways in their own right.[37]

Specifically, we have demonstrated that the redox reactions of 2,5-dimercapto-1,3,4-thiadiazole (DMcT, in the text, we will use DMcT to denote all forms present independent of oxidation state and/or state of protonation), one of the most promising organosulfur compounds as a cathode electroactive material, are dramatically accelerated by the conducting polymer poly(3,4-ethylenedioxythiophene) (PEDOT)-modified glassy carbon electrodes (GCEs) in organic media such as acetonitrile (AN) and propylene carbonate (PC) (Scheme 1).[42,49] Doubly protonated DMcT (DMcT-2H), which possesses two thiol groups, is oxidized to form a disulfide polymer by a two-electron process upon electrochemical oxidation, providing a theoretical capacity of 362 A h kg^{-1}.[36] PEDOT, a polythiophene derivative, has been the subject of numerous studies because of its potential utility in a wide range of applications.[50,51] The presence of the electron-donating oxygen atoms coupled to the thiophene ring at the 3,4-positions provides great electrochemical, chemical, and thermal stability as well as high electronic conductivity over a wide potential range.[52] Furthermore, the p-type doping process starts at more negative potentials when compared to other conducting polymers such as polythiophene, polyaniline, and polypyrrole, and thus PEDOT's window of conductivity has a better overlap with the potentials where the redox reactions of DMcT occur. On the basis of these unique properties, a high electrocatalytic activity of PEDOT towards the redox reactions of DMcT was anticipated and in fact observed.[42]

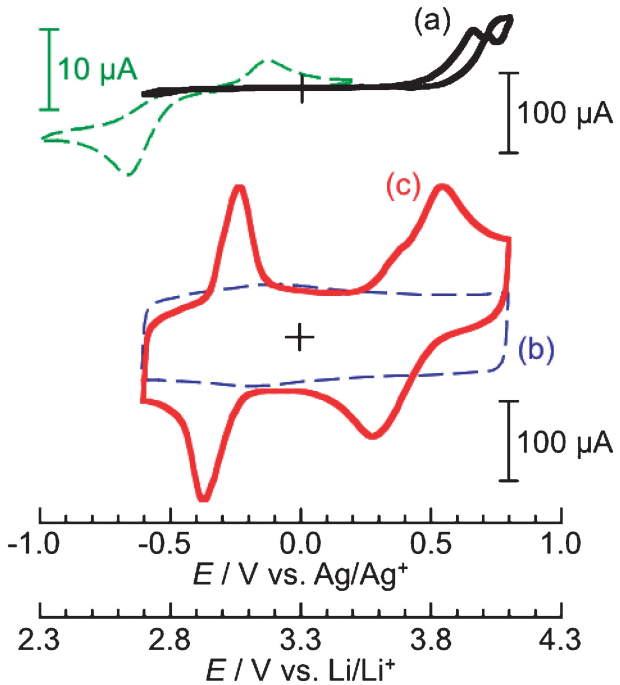

Fig. 10. (a) CVs, recorded over different potential regions, for a 5 mM DMcT-2H solution at a bare GCE in 0.1 M $LiClO_4$/AN. CVs for (b) 0 and (c) 5 mM DMcT-2H solutions at PEDOT film-modified GCEs in 0.1 M $LiClO_4$/AN. The scan rate in all cases was 20 mV s^{-1} [N. Oyama, Y. Kiya, O. Hatozaki, S. Morioka, H. D. Abruña, *Electrochem. Solid-State Lett.* **2003**, *6*, A286. Reproduced by permission of The Electrochemical Society.].

Figure 10a shows a CV for a 5 mM DMcT-2H solution at a bare GCE in an AN solution containing 0.1 M lithium perchlorate ($LiClO_4$) (solid line). An expanded current scale CV for a DMcT solution at a bare GCE in 0.1 M $LiClO_4$/AN is also shown for comparison (dotted line). Figures 10b and 10c show CVs for 0 and 5 mM DMcT-2H solutions at PEDOT film-modified GCEs in 0.1 M $LiClO_4$/AN, respectively. At a

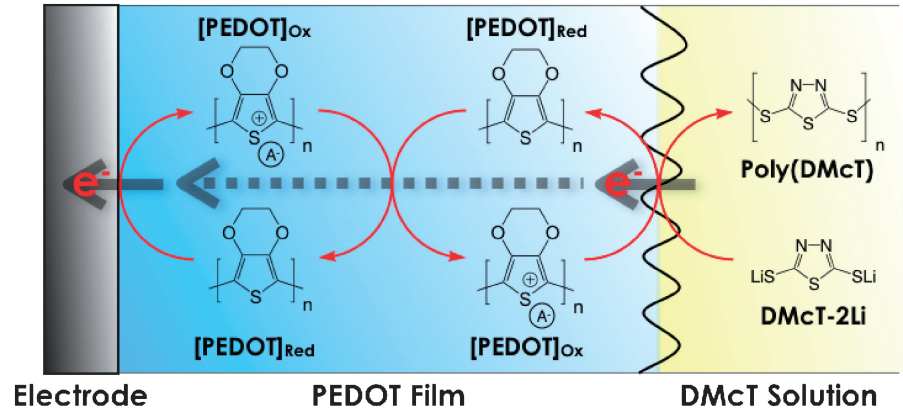

Fig. 11. Electrocatalytic cycle between DMcT and PEDOT. DMcT is oxidized by electrochemically oxidized PEDOT ($[PEDOT]_{Ox}$) during the charging process and PDMcT is reduced by electrochemically reduced PEDOT ($[PEDOT]_{Red}$) during the discharging process [Reprinted with permission from Y. Kiya, G. R. Hutchison, J. C. Henderson, T. Sarukawa, O. Hatozaki, N. Oyama, H. D. Abruña, *Langmuir* **2006**, *22*, 10554. Copyright 2006, American Chemical Society.].

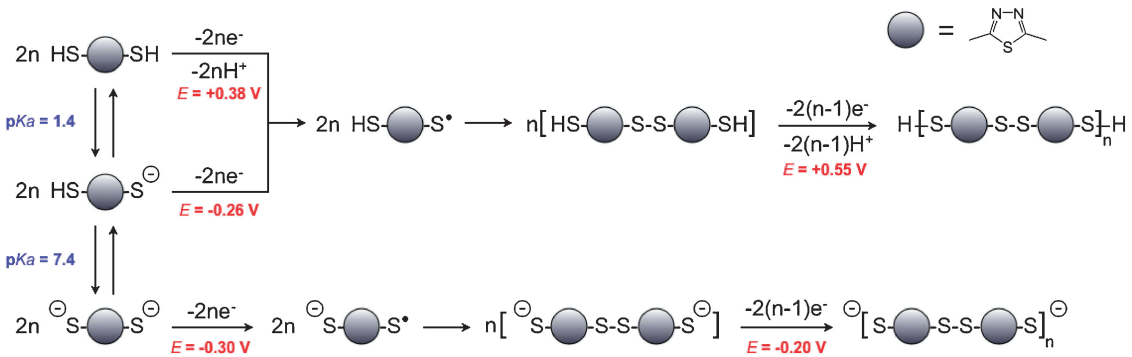

Scheme 2. Proposed anodic reaction scheme for DMcT at a PEDOT-modified GCE in an AN solution [Reprinted with permission from Y. Kiya, G. R. Hutchison, J. C. Henderson, T. Sarukawa, O. Hatozaki, N. Oyama, H. D. Abruña, *Langmuir* **2006**, *22*, 10554. Copyright 2006, American Chemical Society.].

PEDOT modified GCE, the DMcT-2H solution exhibited two clearly developed redox couples due to the redox reactions of DMcT-2H, both absent at an unmodified GCE, as a result of the electrocatalytic effect of PEDOT over the potential range from −0.60 to +0.80 V vs. Ag/Ag^+. Spectroelectrochemical studies revealed that the electrocatalytic effect is based on the electron-exchange reactions between DMcT and PEDOT as depicted in Fig. 11.[53] DMcT in an electrolyte solution is oxidized to its polymeric form (PDMcT) by electrochemically oxidized PEDOT ($[PEDOT]_{Ox}$) during the charging process, and PDMcT is reduced back to DMcT monomer by electrochemically reduced PEDOT, $(PEDOT)_{Red}$ during the discharging process.

The redox behavior of DMcT at PEDOT-modified GCEs was also investigated in detail by means of CV, acid–base chemistry, and electrochemical quartz crystal microbalance (EQCM) techniques in order to elucidate the redox reaction mechanism.[46] It was revealed that, while the thermodynamics of the redox reactions of DMcT are strongly dependent upon the basicity or acidity of the solution employed, all forms of DMcT (Scheme 1) are electrocatalyzed at PEDOT film-coated GCEs. For an anodic potential scan, DMcT-2H and singly protonated DMcT (DMcT-1H) are oxidized to the protonated dimer at +0.38 and −0.26 V vs. Ag/Ag^+, respectively, and doubly deprotonated DMcT ($DMcT^{2-}$) is oxidized to the deprotonated dimer at −0.30 V. The dimerization of DMcT-1H occurs not only at the surface of a PEDOT film but also inside the film. The protonated and deprotonated dimers are oxidized to the polymer at +0.55 and −0.20 V, respectively. For a cathodic scan, DMcT polymer is reduced back to the protonated dimer at +0.35 V (involving a proton-transfer reaction) and the protonated dimer is reduced back to DMcT-2H at +0.25 V and to DMcT-1H at −0.32 V. Moreover, DMcT polymer is reduced back to $DMcT^{2-}$ via the deprotonated dimer over the potential range from −0.20 to −1.20 V when proton transfer is not involved. Furthermore, the redox reactions of DMcT involve the chemical conproportionation of DMcT polymer and monomer to generate dimers as previously suggested.[54] The proposed anodic and cathodic reactions are summarized in Schemes 2 and 3, respectively.[46] The potentials reported are the peak potentials for the reactions and referenced against a Ag/Ag^+ electrode.

Furthermore, we have quantitatively analyzed the electron-exchange reaction between DMcT and PEDOT via rotating-disk electrode (RDE) voltammetry.[53] The analysis was focused on the charge transfer from $(PEDOT)_{Red}$ (at the modified electrode) to DMcT dimer (diDMcT) (in solution) in order to avoid any complications due to the deposition process of DMcT

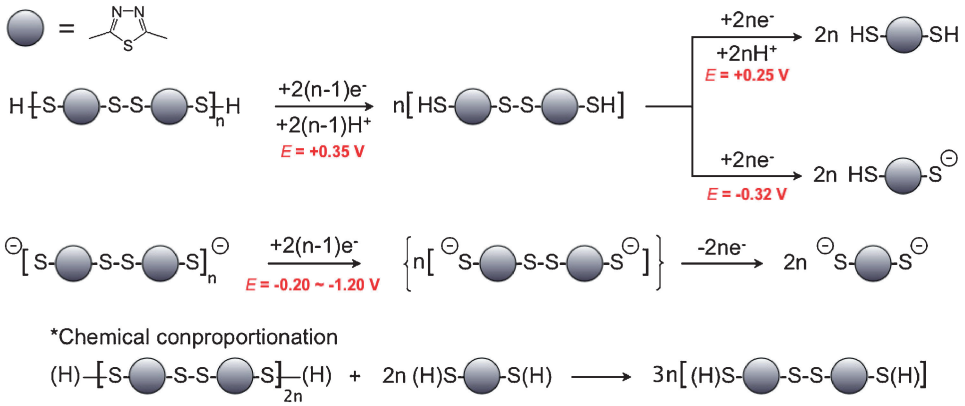

Scheme 3. Proposed cathodic reaction scheme for DMcT at a PEDOT-modified GCE in an AN solution [Reprinted with permission from Y. Kiya, G. R. Hutchison, J. C. Henderson, T. Sarukawa, O. Hatozaki, N. Oyama, H. D. Abruña, *Langmuir* **2006**, *22*, 10554. Copyright 2006, American Chemical Society.].

polymer involved in the electrochemical oxidation. The kinetic model employed to estimate the charge-transfer rate was based on the analysis previously proposed by Savéant and co-workers, which takes into account charge propagation (a self-exchange reaction) in a polymer film (PEDOT) on an electrode surface and diffusion of a substrate (diDMcT) through the polymer film.[55] Thus, it is appropriate to our system which employs a multimolecular layer film on an electrode. On the basis of this kinetic model, the overall process of our system has shown to be controlled by the catalytic reaction and the diffusion of diDMcT in the film (so-called "SR" model). The second-order rate constant for the charge-transfer reaction was estimated as 32 M^{-1} s^{-1}. This rate constant is significantly greater than that previously obtained for the charge-transfer reaction from the reduced form of polyaniline (PAn) to diDMcT (0.03 M^{-1} s^{-1}) as well as the constants between other orgnosulfur compounds and reduced PAn estimated via UV–vis spectroscopy,[56] establishing the high electrocatalytic activity of PEDOT towards the redox reactions of DMcT. Moreover, a comparison of the standard rate constants, k^0, for the DMcT/diDMcT redox couple obtained at bare and PEDOT film-modified GCEs indicates that the redox reaction is accelerated by ca. 12000 times at the PEDOT film-coated GCE. These results demonstrate that the use of conducting polymers, such as PEDOT, as efficient electrocatalysts for the redox reactions of DMcT, is a promising strategy to utilize organosulfur compounds as an energy-storage material in lithium-ion rechargeable batteries.

We have also evaluated the charge/discharge performance of composite cathode films composed of DMct polymer (PDMcT) and PEDOT in a mixed solution of ethylene carbonate (EC) and diethyl carbonate (DEC) (1:3 wt % ratio) containing 1.0 M lithium tetrafluoroborate ($LiBF_4$) at a rate of 0.1 C for both charge and discharge.[49] Cut-off potentials for charging and discharging reactions were set at 3.7 and 2.0 V (vs. Li/Li^+), respectively. A prototype lithium-battery cell was fabricated with a PDMcT/PEDOT composite cathode, a lithium-metal anode, polyolefin porous films (for separators), current collectors (carbon-coated aluminum for the cathode and copper for the anode), and Teflon-coated metal plates. The composite cathode film was prepared from a slurry composed of PDMcT, PEDOT, carbon black (CB), and polyvinylidene fluoride (PVdF). PDMcT and PEDOT were obtained by the chemical polymerization of DMcT and EDOT monomers by using iodine and copper(II) tetrafluoroborate, respectively, as oxidizing agents.[49] Figure 12a presents potential profiles for the first charge/discharge cycle for a PDMcT/PEDOT (1:1 mol ratio) composite cathode in a EC:DEC (1:3 wt % ratio) solution containing 1.0 M $LiBF_4$. At the first discharge process, the composite cathode exhibited 205 A h kg^{-1} (based on the electroactive mass) with a potential plateau at 2.8 V vs. Li/Li^+ (corresponding to 574 W h kg^{-1} of energy density) due to the electrocatalytic reduction of PDMcT. However, the capacity obtained at the first recharge was only 88 A h kg^{-1},

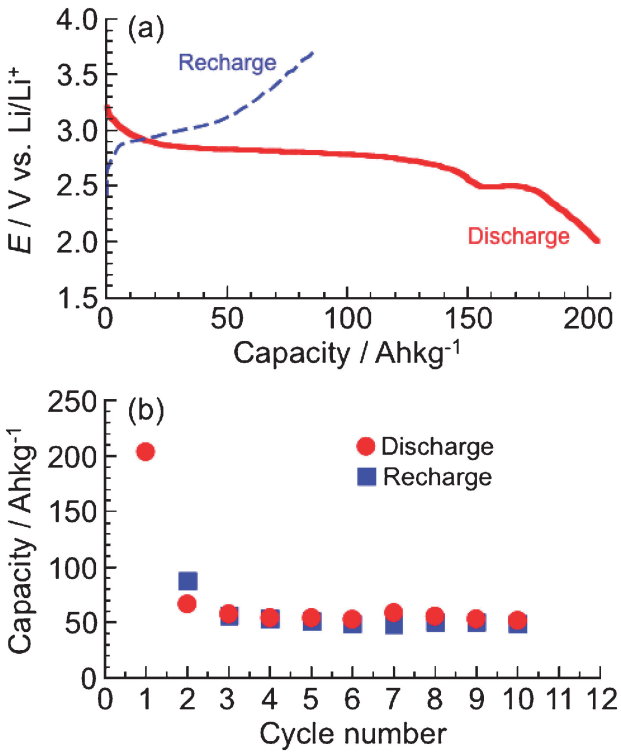

Fig. 12. (a) Potential profiles for the first charge/discharge cycle and (b) charge/discharge cycle durability for a PDMcT/PEDOT composite cathode in a 1.0 M $LiBF_4$/EC:DEC (1:3 wt % ratio) solution.

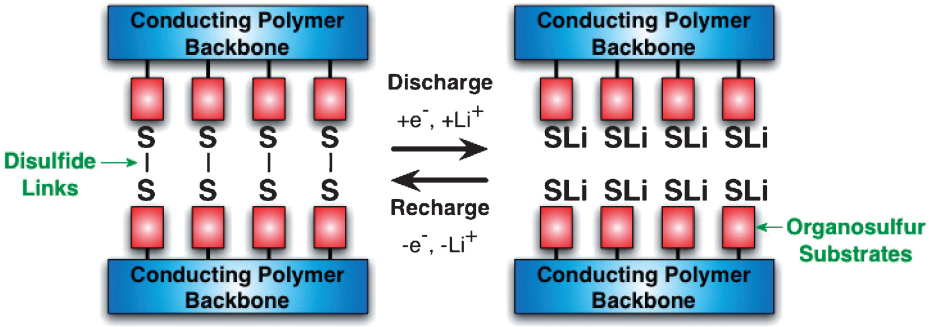

Fig. 13. Rocking-chair type system based upon a thiolate/disulfide redox reaction. Disulfide moieties are covalently bonded to conducting polymer π-backbones.

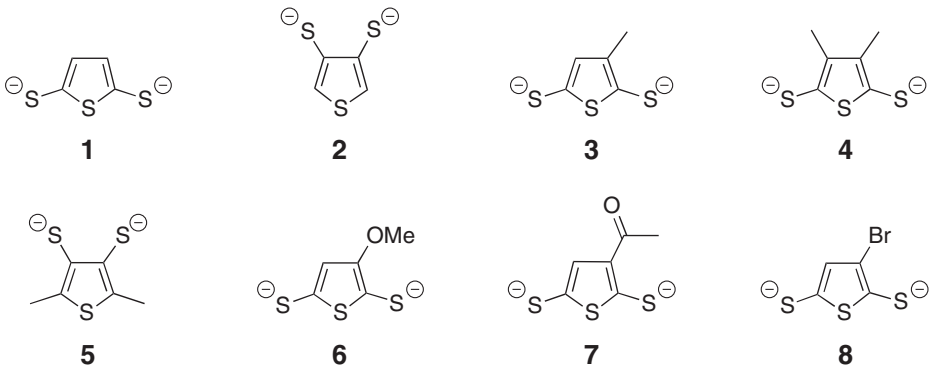

Fig. 14. Organosulfur compounds synthesized and studied, including a variety of electron-donating and electron-withdrawing substituents on the basic thiophene-2,5-bis(thiolate) (TBT) **1** structure. The acetyl-protected molecules are synthesized to prevent disulfide formation, and the thiolates are generated in-situ before electrochemical measurements.

and the discharge capacity reached ca. 50 A h kg^{-1} after the third cycle (Fig. 12b). Results obtained from CV and scanning electron microscopy (SEM) studies indicated that the capacitive loss is mainly due to dissolution of reduction products of PDMcT such as DMcT monomer into the electrolyte solution. Therefore, while a PDMcT/PEDOT composite system exhibited great potential as a high energy density cathode for lithium/lithium-ion batteries as a result of the electrocatalytic effect of PEDOT towards PDMcT, its practical application will require a breakthrough in the charge/discharge cyclability.

2.3 From Composite to Hybrid Materials. In order to prevent dissolution of thiolate monomers (e.g., DMcT monomer) following reduction of the disulfide polymers, we have designed, synthesized, and characterized new organic hybrid materials, in which an organosulfur (thiolate) segment is covalently bonded to a conducting polymer backbone as shown in Fig. 13. In these hybrid materials, soluble organosulfur segments never leach out of the cathode film into the electrolyte solution due to the connection, via a covalent bond, to an insoluble conducting polymer chain. In particular, the thiolate segments and conducting polymer π-backbones were designed to incorporate both an energy storage site (a lithium-ion doping/dedoping site) and an electrocatalyst for the thiolate segments, respectively. Moreover, since the π-conjugated chains work as electronically conductive pathways, the hybrid materials should also be electronically conductive. Designing a conducting electroactive material offers a number of advantages in practical applications (e.g., reducing the amount of carbon materials such as CB required in a cathode film).

The thiolate segment for the energy storage site has to be electrocatalyzed by the π-conjugated backbone segment (because of the sluggish charge-transfer kinetics), while also possessing a synthetically tunable point for attachment. Although PEDOT exhibits high electrocatalytic activity towards DMcT, the thiadiazole ring in DMcT does not have a point of attachment. In order to gain an electrocatalytic effect for new thiolate compounds, instead of DMcT, thermodynamic relationships between thiolate compounds and PEDOT were investigated via computational modeling in order to find the appropriate combination allowing for such electrocatalytic reactions. On the basis of the electrochemical and computational understanding of the thermodynamics of the electrocatayltic cycle between DMcT and PEDOT, it would appear that any organosulfur compound with a highest-occupied molecular orbital (HOMO) level between the neutral PEDOT HOMO level and cationic PEDOT singly occupied molecular orbital (SOMO) level should exhibit anodic electrocatalysis by PEDOT. Similarly, compounds with a LUMO level approximating the PEDOT HOMO level should show cathodic electrocatalysis by PEDOT. Figure 14 shows dimercaptothiophene (thiophene-2,5-bis(thiolate), TBT) and its derivatives with a variety of functional groups (electron-donating and electron-withdrawing) and regiochemistries investigated in our studies.[47] On the basis of the results obtained from computational studies, TBT and its derivatives should have electronic states allowing the electrocatalysis by PEDOT towards the redox re-

actions. Moreover, since TBT possesses synthetically tunable points at the 3,4-positions, it is possible to incorporate TBT via covalent bonds to a PEDOT π-conjugated chain.

Indeed, investigation of the redox behavior of the TBT family (Fig. 14) at PEDOT film-coated GCEs revealed that the redox reactions of all the compounds are electrocatalyzed at a PEDOT film-coated GCE as predicted by the computational studies, although some exhibited higher energy output than others.[47] Figures 15b and 15c show representative CVs for 1 mM TBT **1** at a bare GCE (Fig. 15b) and a PEDOT film-coated GCE (obtained at the fifth cycle, Fig. 15c) in a 0.1 M $LiClO_4$/AN solution. Figure 15a shows a CV for a PEDOT film-coated GCE in a 0.1 M $LiClO_4$/AN solution for comparison. For the oxidation of TBT at a PEDOT film-modified GCE, the onset potential shifted towards negative values and the current response increased relative to a bare GCE. On the other hand, for the reduction, the peak potential obtained at a bare GCE shifted from -1.06 to -0.85 V ($\Delta E = +210$ mV), with an increase in the current response, at a PEDOT film-modified GCE. Furthermore, a composite film of TBT polymer (PTBT) and PEDOT with CB and PVdF modified on a GCE showed a large cathodic current, corresponding to the disulfide cleavage of PTBT, in a 0.1 M $LiClO_4$/AN solution at the first reduction in the potential region from 2.6 to 2.0 V vs. Li/Li^+ as a result of electrocatalysis by PEDOT (data not shown). PTBT was chemically prepared by using iodine as an oxidizing agent and the composite film was prepared by casting a 1-methyl-2-pyrrolidinone (NMP) dispersion containing PTBT, CB, and PVdF. The reaction efficiency of the disulfide reduction at the first reduction was found to be nearly 100%, indicating high electrocatalytic activity of PEDOT towards the redox reactions of PTBT.

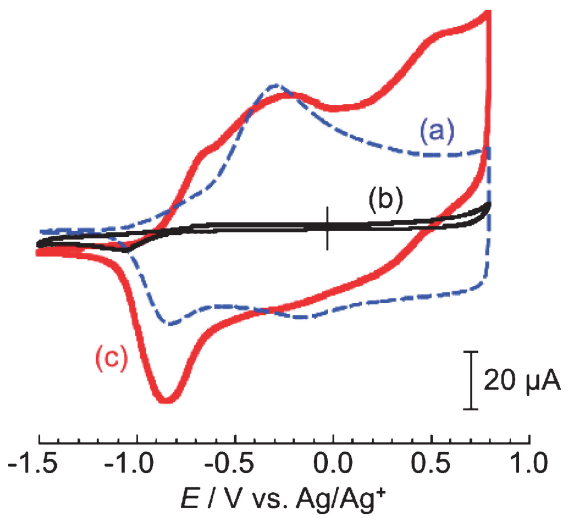

Fig. 15. (a) CV for a PEDOT film-coated GCE in 0.1 M $LiClO_4$/AN. Representative CVs for 1 mM TBT **1** at (b) bare and (c) PEDOT film-coated GCEs in 0.1 M $LiClO_4$/AN. The scan rate in all cases was 20 mV s^{-1}.

We showed that PEDOT exhibits electrocatalytic activity towards the redox reactions of TBT which, in turn, possesses synthetically tunable points for coupling to PEDOT. Thus, our current work has focused on the synthesis of novel PEDOT-based hybrid materials possessing TBT segments as an energy storage site through the synthetic route shown in Scheme 4. 2,3-Dihydrothieno[3,4-*b*]-1,4-dioxn-2-yl-methanol (EDOT-MeOH) **9** bearing a hydroxy group was tosylated. 3-Bromo-2,5-bis(alkylthio)thiophene **11** was lithiated and converted to the Grignard with $MgBr_2 \cdot OEt_2$ and then added to the tosylated EDOT **10** in ether with a catalytic amount of CuBr·DMS to give the hybrid material, TBT-attached EDOT **13**. In order to protect the thiolate functionality, either a methyl or *tert*-butyl substituent was employed as a protecting group. Polymerization of the hybrid material and removal of the protecting groups is currently being investigated to obtain a PEDOT π-conjugated chain with electroactive TBT segments **14**.

Summary

In this account, we presented our current work on electrochemical energy generation and storage (i.e., fuel cells and lithium-ion batteries).

For fuel cell research, new types of CO tolerant electrocatalysts of ordered intermetallic phases exhibited far superior performance to Pt and Pt–Ru alloys in terms of onset potential and current density in FA oxidation. High-throughput experimental techniques, using thin film composition spreads, have been shown to yield important leads for new promising electrocatalysts. In addition, in the use of laminar flow fuel cells, we have demonstrated that we could overcome low power densities by employing dual electrolyte solutions with different pH containing O_2 and H_2. We have shown that the use of ordered intermetallic phases, the development of combinatorial methods for high-throughout screening of promising electrocatalysts, and the use of membraneless microchannel fuel cells, employing dual electrolyte laminar flows, offer viable avenues of

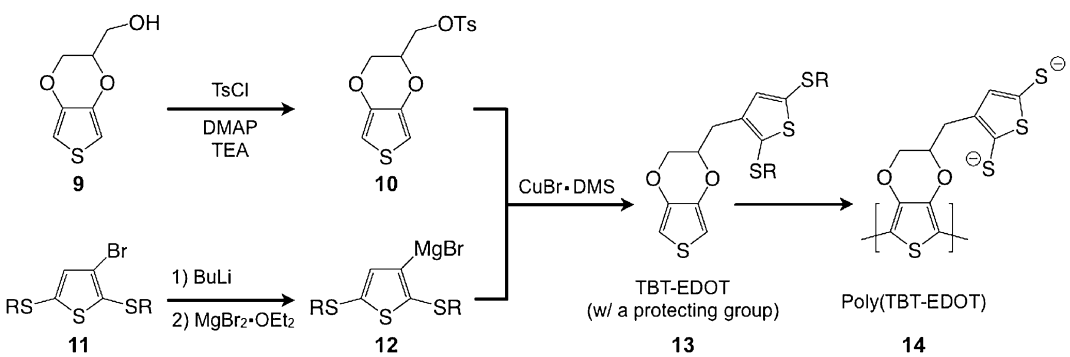

Scheme 4. Synthesis of TBT-attached PEDOT.

research in the quest to develop PEMDFCs with desired performance and reliability.

Our lithium-ion battery research has focused on the development of high-energy cathodes based on new organosulfur-based materials. Their potentially high capacities, the global abundance of sulfur as well as lower cost to manufacture make them ideal for large scale applications. While we have been able to dramatically accelerate the charge-transfer kinetics of organosulfur compounds, further research is required in order to improve the charge/discharge cyclability. We have designed novel organosulfur-based hybrid materials in which thiolate compounds, as an energy-storage segment, are attached to a conducting polymer π-backbone. We are currently determining the most promising family of materials.

The fuel cell research was supported in part by the Basic Energy Sciences Division of the Department of Energy (Nos. DE-FG02-87ER45298 and DE-FG02-03ER46072), Army Research Office (ARO) (No. DAAD19-03-C-0100), the Cornell Center for Materials Research (CCMR), and the National Science Foundation (NSF) (No. ACT-0346377). The μ-fabrication of the planar membraneless microchannel fuel cell was performed in part at the Cornell Nanoscale Facility (a member of the National Nanotechnology Infrastructure Network) which is supported by the NSF (No. ECS-0335765), its users, Cornell University, and Industrial Affiliates. The lithium-ion battery research was supported in part by Fuji Heavy Industries Limited and CCMR.

References

1 M. Z. Jacobson, W. G. Colella, D. M. Golden, *Science* **2005**, *308*, 1901.
2 M. Granovskii, I. Dincer, M. A. Rosen, *J. Power Sources* **2006**, *157*, 411.
3 K. Sopian, W. R. W. Daud, *Renewable Energy* **2006**, *31*, 719.
4 M. Winter, R. J. Brodd, *Chem. Rev.* **2004**, *104*, 4245.
5 A. S. Aricó, S. Srinivasan, V. Antonucci, *Fuel Cells* **2001**, *1*, 133.
6 H. S. Liu, C. J. Song, L. Zhang, J. J. Zhang, H. J. Wang, D. P. Wilkinson, *J. Power Sources* **2006**, *155*, 95.
7 W. M. Qian, D. P. Wilkinson, J. Shen, H. J. Wang, J. J. Zhang, *J. Power Sources* **2006**, *154*, 202.
8 M. Arenz, V. Stamenkovic, T. J. Schmidt, K. Wandelt, P. N. Ross, N. M. Markovic, *Chem. Phys. Chem. Phys.* **2003**, *5*, 4242.
9 M. Götz, H. Wendt, *Electrochim. Acta* **1998**, *43*, 3637.
10 L. A. Kibler, A. M. El-Aziz, D. M. Kolb, *J. Mol. Catal. A: Chem.* **2003**, *199*, 57.
11 E. Casado-Rivera, Z. Gál, A. C. Angelo, C. Lind, F. J. DiSalvo, H. D. Abruña, *ChemPhysChem* **2003**, *4*, 193.
12 E. Casado-Rivera, D. J. Volpe, L. Alden, C. Lind, C. Downie, T. Vazquez-Alvarez, A. C. Angelo, F. J. DiSalvo, H. D. Abruña, *J. Am. Chem. Soc.* **2004**, *126*, 4043.
13 C. Roychowdhury, F. Matsumoto, P. F. Mutolo, H. D. Abruña, F. J. DiSalvo, *Chem. Mater.* **2005**, *17*, 5871.
14 C. Roychowdhury, F. Matsumoto, V. B. Zeldovich, S. C. Warren, P. F. Mutolo, M. Ballesteros, U. Wiesner, H. D. Abruña, F. J. DiSalvo, *Chem. Mater.* **2006**, *18*, 3365.
15 L. R. Alden, C. Roychowdhury, F. Matsumoto, D. K. Han, V. B. Zeldovich, H. D. Abruña, F. J. Disalvo, *Langmuir* **2006**, *22*, 10465.
16 L. R. Alden, D. K. Han, F. Matsumoto, H. D. Abruña, F. J. DiSalvo, *Chem. Mater.* **2006**, *18*, 5591.
17 M. Prochaska, J. Jin, D. Rochefort, L. Zhuang, F. J. DiSalvo, H. D. Abruña, R. B. van Dover, *Rev. Sci. Instrum.* **2006**, *77*, 054104.
18 H. L. Maynard, J. P. Meyers, *J. Vac. Sci. Technol., B* **2002**, *20*, 1287.
19 J. S. Wainright, R. F. Savinell, C. C. Liu, M. Litt, *Electrochim. Acta* **2003**, *48*, 2869.
20 J. L. Cohen, D. A. Westly, A. Pechenik, H. D. Abruña, *J. Power Sources* **2005**, *139*, 96.
21 L. W. Niedrach, D. W. Mckee, J. Paynter, I. F. Danzig, *Electrochem. Technol.* **1967**, *5*, 318.
22 M. Watanabe, S. Motoo, *J. Electroanal. Chem.* **1975**, *60*, 275.
23 D. S. Gottesfeld, private communication, *MTI Micro Fuel Cells*, **2003**.
24 J. L. Cohen, D. J. Volpe, D. A. Westly, A. Pechenik, H. D. Abruña, *Langmuir* **2005**, *21*, 3544.
25 J. M. Tarascon, M. Armand, *Nature* **2001**, *414*, 359.
26 M. S. Whittingham, *Chem. Rev.* **2004**, *104*, 4271.
27 R. Koksbang, J. Barker, H. Shi, M. Y. Saïdi, *Solid State Ionics* **1996**, *84*, 1.
28 K. S. Kang, Y. S. Meng, J. Breger, C. P. Grey, G. Ceder, *Science* **2006**, *311*, 977.
29 A. K. Padhi, K. S. Nanjundaswamy, J. B. Goodenough, *J. Electrochem. Soc.* **1997**, *144*, 1188.
30 M. S. Whittingham, Y. N. Song, S. Lutta, P. Y. Zavalij, N. A. Chernova, *J. Mater. Chem.* **2005**, *15*, 3362.
31 Y. Idota, T. Kubota, A. Matsufuji, Y. Maekawa, T. Miyasaka, *Science* **1997**, *276*, 1395.
32 P. Poizot, S. Laruelle, S. Grugeon, L. Dupont, J. M. Tarascon, *Nature* **2000**, *407*, 496.
33 R. A. Huggins, *Solid State Ionics* **2002**, *152–153*, 61.
34 Y. P. Wu, E. Rahm, R. Holze, *J. Power Sources* **2003**, *114*, 228.
35 K. Zaghib, K. Kinoshita, *J. Power Sources* **2004**, *125*, 214.
36 M. Liu, S. J. Visco, L. C. De Jonghe, *J. Electrochem. Soc.* **1991**, *138*, 1891.
37 P. Novak, K. Muller, K. S. V. Santhanam, O. Haas, *Chem. Rev.* **1997**, *97*, 207.
38 L. Yu, X. H. Wang, J. Li, X. B. Jing, F. S. Wang, *J. Power Sources* **1998**, *73*, 261.
39 J. S. Cho, S. Sato, S. Takeoka, E. Tsuchida, *Macromolecules* **2001**, *34*, 2751.
40 H. Uemachi, Y. Iwasa, T. Mitani, *Electrochim. Acta* **2001**, *46*, 2305.
41 L. J. Xue, J. X. Li, S. Q. Hu, M. X. Zhang, Y. H. Zhou, C. M. Zhan, *Electrochem. Commun.* **2003**, *5*, 903.
42 N. Oyama, Y. Kiya, O. Hatozaki, S. Morioka, H. D. Abruña, *Electrochem. Solid-State Lett.* **2003**, *6*, A286.
43 X. G. Yu, J. Y. Xie, J. Yang, H. J. Huang, K. Wang, Z. S. Wen, *J. Electroanal. Chem.* **2004**, *573*, 121.
44 S. R. Deng, L. B. Kong, G. Q. Hu, T. Wu, D. Li, Y. H. Zhou, Z. Y. Li, *Electrochim. Acta* **2006**, *51*, 2589.
45 M. Amaike, T. Iihama, *Synth. Met.* **2006**, *156*, 239.
46 Y. Kiya, G. R. Hutchison, J. C. Henderson, T. Sarukawa, O. Hatozaki, N. Oyama, H. D. Abruña, *Langmuir* **2006**, *22*, 10554.
47 Y. Kiya, J. C. Henderson, G. R. Hutchison, H. D. Abruña,

J. Mater. Chem. **2007**, in press. doi: 10.1039/b707235j.
48 A. G. MacDiarmid, *Synth. Met.* **2001**, *125*, 11.
49 Y. Kiya, A. Iwata, T. Sarukawa, J. C. Henderson, H. D. Abruña, *J. Power Sources* **2007**, in press. doi: 10.1016/j.jpowsour.2007.04.086.
50 G. Heywang, F. Jonas, *Adv. Mater.* **1992**, *4*, 116.
51 M. Dietrich, J. Heinze, *J. Electroanal. Chem.* **1994**, *369*, 87.
52 Q. Pei, G. Zuccarello, M. Ahlskog, O. Inganas, *Polymer* **1994**, *35*, 1347.
53 Y. Kiya, O. Hatozaki, N. Oyama, H. D. Abruña, *J. Phys. Chem. C* **2007**, in press. doi: 10.1021/jp073486f.
54 T. Tatsuma, Y. Yokoyama, D. A. Buttry, N. Oyama, *J. Phys. Chem. B* **1997**, *101*, 7556.
55 C. P. Andrieux, J. M. Dumas-Bouchiat, J. M. Savéant, *J. Electroanal. Chem.* **1982**, *131*, 1.
56 T. Tatsuma, F. Matsui, E. Shouji, N. Oyama, *J. Phys. Chem.* **1996**, *100*, 14016.

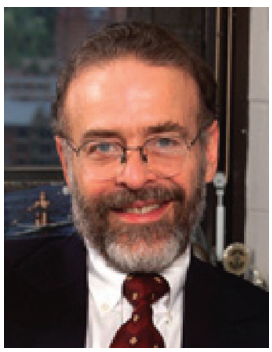

Professor Héctor D. Abruña, Emile M. Chamot Professor of Chemistry and Chair, completed his graduate studies with Royce W. Murray and Thomas J. Meyer at the University of North Carolina at Chapel Hill in 1980 and was a postdoctoral research associate with Allen J. Bard at the University of Texas at Austin. After a brief stay at the University of Puerto Rico, he came to Cornell in 1983. Professor Abruña is the recipient of a Presidential Young Investigator Award, an Alfred P. Sloan Foundation Research Fellowship, a John S. Guggenheim Fellowship, the Tajima Prize of the International Society of Electrochemistry, a J. W. Fulbright Senior Research Fellowship, and an Iberdrola Fellowship. Most recently, he has been named a fellow of the American Academy of Arts and Sciences, the American Association for the Advancement of Science (AAAS), and the 2007 recipient of the Electrochemistry Award of the American Chemical Society. His research effort takes an interdisciplinary approach to the study of electrochemical phenomena by employing electrochemical techniques to probe a variety of chemical systems, while also using synthesis and computational modeling in order to address problems of electrochemical interest. Specific areas of current interest include fuel cells, energy-storage devices, molecular electronics, and organic light-emitting diodes (OLEDs).